Published in final edited form as:
Proteins. 2011 February ; 79(2): 537–546. doi:10.1002/prot.22901.

A mechanism by which binding of the broadly neutralizing antibody b12 unfolds the inner domain *α*1 helix in an engineered HIV-1 gp120

Ali Emileh and **Cameron F. Abrams***
Department of Chemical and Biological Engineering, Drexel University, 3141 Chestnut St., Philadelphia, PA 19104

Abstract

Using all-atom simulations, we examine the role of the I109C/Q428C disulfide "stitch" in altering the conformational distribution of engineered HIV-1 gp120 core relevant for binding of the broadly neutralizing recombinant antibody b12. In particular, we propose that the I109C/Q428C stitch results in a conformational distribution favoring an unfolded inner-domain *α*1-helix upon binding of b12. Using Targeted Molecular Dynamics (TMD), we show that folded *α*1 in the b12-bound conformation of gp120 is stable both with and without the stitch, but that with folded *α*1, the stitch requires an orientation of the *β*20/*β*21 sheet that is sterically incompatible with b12 binding. Forcing *β*20/*β*21 into the orientation displayed by the b12-bound conformation after folding *α*1 with the stitch intact results in partial unfolding of *α*1, whereas without the stitch, *β*20/*β*21 reorientation does not affect the conformation of *α*1. These findings collectively support the hypothesis that the disulfide stitch shifts the conformational distribution of *α*1 to the unfolded state, meaning an unfolded *α*1 is not a strict requirement of the b12-bound conformational ensemble of gp120's lacking the I109C/Q428C stitch.

INTRODUCTION

Human immunodeficiency virus (HIV) is decorated on its surface by spike-like glycoprotein complexes which mediate viral entry into cells and are therefore targets for developing entry inhibitors and vaccines (1–3). Each envelope spike is a trimer of dimers of transmembrane gp41 and the highly glycosylated gp120 which is non-covalently linked to gp41 (3,4). The first crystallographically resolved conformation of HIV-1 gp120 showed the deglycosylated core gp120 in a ternary complex with a soluble form of its cognate receptor CD4 and an antibody surrogate (17b) for a mandatory coreceptor (5–7) (Figure 1a). In this "activated" state, gp120 assumes a two-domain topology where the inner and outer domains each contribute two *β* strands to the so-called "bridging sheet" which is the site of coreceptor binding (5). The inner domain mediates association with gp41 (8). The two domains and the bridging sheet come together around a small but functionally important cavity which is capped by F43 of bound CD4 (5).

Binding of CD4 to gp120 is accompanied by an unusually large negative change in entropy ($-T\Delta S \approx$ 38-44 kcal/mol at 37°C) which indicates structuring of gp120 out of more flexible unliganded conformations (2,9–11). About half of this structural rearrangement can be attributed to folding of the bridging sheet (9). Despite the absence of an unliganded HIV gp120 structure, it has been argued that the inner domain must go through major

* cfa22@drexel.edu.

conformational changes upon CD4 binding, possibly involving independent movements of distinct structural motifs (11). One possible structural basis for such movements can be inferred from the structure of gp120 in complex with the Fab fragment of the recombinant broadly neutralizing antibody b12 (10)(Figure 1b). Relative to CD4, b12 binding to gp120 is associated with an almost seven times smaller negative change in entropy (12). The small entropic penalty gp120 pays upon binding b12 is thought to be the key to b12's unique neutralizing ability because it renders the “conformational masking” defense of gp120 less effective (12). However, the lack of conformational fixation also works against crystallization of a gp120/b12 complex. To circumvent this, Zhou *et al*. introduced various stabilizing mutations in the gp120 sequence which limited its conformational flexibility (10): four cysteine mutations which created two interdomain disulfide bridges, and five so-called “pocket filling” mutations, all of which enhanced structural stability of the activated conformation. When considering the CD4-bound activated conformation, the engineered disulfide at I109C/Q428C “stitches” the tip of the loop connecting the β20/β21 strands of the bridging sheet to the α1 helix of the inner domain (Figure 1a).

In the b12-bound conformation, the β20/β21 strand is flipped compared to the CD4-bound state and the hydrogen bond registry is shifted by one or two residues. Also the β2/β3 part of the bridging sheet is completely absent from the crystal structure, suggesting it is unstructured (10). The outer domain, excluding the β20/β21 excursion, has essentially the same structure in the two conformations. In contrast with the CD4-bound inner domain, the α1 helix is almost completely unfolded in the b12-bound structure, except for a turn near its C-terminus. Evidently, b12 binding abolishes the ability of gp120 to form the bridging sheet, as is supported by b12/17b competition assays (13), and it makes contacts with the β20/β21 strands but does not contact any residues in the inner domain (10). It is worth noting that within the impressive collection of gp120 conformations crsytallographically resolved to date (5,8,11), only two highly engineered gp120's have an unfolded α1 and these are the ones in complex with b12 and b13 (a closely b12-related mAb with lower neutralization ability (8)). It is therefore puzzling why there is an apparent link between b12 binding and an unfolded α1-helix.

The purpose of this paper is to use all-atom simulation to explore the hypothesis that unfolding of the α1 helix in engineered gp120's is likely favored by the simultaneous presence of the disulfide mutation that stitches α1 to the β20/β21 half of the bridging sheet and b12 binding which, through this stitch, couples the movement of β20/β21 to α1. We characterize the extent to which the presence of the disulfide bridge between β20/β21 and α1 couples their movements together and we demonstrate that in the absence of this disulfide stitch, the helical conformation of α1 can remain unaltered upon b12 binding.

METHODS

All structural manipulations and molecular dynamics simulations are performed using the software package NAMD 2.7b1 (14) and the CHARMM22 force-field (15,16). HxBc2 strain gp120 core coordinates for the activated conformation were taken from the ternary crystal structure of gp120/CD4/17b (PDB 1GC1). Core is deglycosylated with GAG replacements in place of V1/V2 and V3 loops and lacks some residues from the N and C-termini (5). Initial coordinates for the b12-bound conformation of core gp120 were taken from the crystallographic data of the gp120/b12 complex (PDB code 2NY7). Compared to the wild-type activated structure of gp120, this structure lacks some parts of β2/β3 and the base of the V1/V2 loop in addition to the V4 loop. Missing residues were modeled *in silico* as an unstructured loop. We refer to this structure as “the stitched conformation” or “DS1”. Using the same crystal structure, we reverted the I109C/Q428C pair of mutations to arrive at the

"DS1F123" sequence (10) which lacks this stitching disulfide bridge. We refer to this latter structure as "the non-stitched conformation" or "DS1*".

In all production MD runs, the system was solvated in a TIP3P (17) water box ($83 \times 89 \times Å^3$ for DS1 and $83 \times 88 \times 81$ $Å^3$ for DS1*), which resulted in a system of ≈56000 atoms. Neutralizing Na+ and Cl- ions were added (total concentration of NaCl 0.025 M). A 2 fs timestep was used in the integrations. The temperature was set to 310 K by coupling all the non-hydrogen atoms to a Langevin thermostat with a friction constant of 5 ps^{-1}. Non-bonded interactions were cut off beyond 9 Å and smoothed to zero beginning from 8 Å. PME long-range-electrostatics with a grid spacing of 1 Å were used and all bonds involving hydrogens were constrained using RATTLE (18). Equilibration runs were performed using a Nosé-Hoover Langevin piston (19,20) at 1 bar. All the initial configurations were first subjected to 20000 steps of minimization and then 20 ns of equilibration. The end results of these initial equilibrations were used as starting points for targeted molecular dynamics (TMD) runs.

In TMD, the protein is driven from a given initial conformation to a given target conformation through the application of a time-dependent restraining force (21). As implemented in NAMD, this steering force is applied to the system through a potential of the following form:

$$U_{\mathrm{TMD}}(t) = \frac{k}{2N}[\mathrm{RMSD}(t) - \mathrm{RMSD}^*(t)]^2 \quad (1)$$

where RMSD(t) is the instantaneous best-fit root-mean-squared deviation from the target conformation and RMSD*(t) evolves linearly from the measured initial value to the final desired value of zero. *k* is the force constant and *N* is the total number of atoms being forced. Our first goal was to generate a folded $\alpha 1$ helix as in the activated conformation with as many of the inner/outer domain contacts in place and as few perturbations in the outer domain and the F43 pocket residues as possible. All the heavy atoms of the $\alpha 1$ helix (residues 100-116) and a small part of the strand connecting the $\beta 3$ and $\beta 4$ motifs (residues 208-212) were subjected to TMD forces. This part of the strand forms a small but very stable β-sheet with lower portions of $\alpha 1$ and preliminary results showed that when $\alpha 1$ is forced through TMD into an α-helix, this strand is deformed and moves between the outer and inner domains and prevents formation of some crystallographic contacts (compared to the activated structure) between the two domains. In addition, all the heavy atoms of the $\alpha 5$ helix were used as an "anchor" to place $\alpha 1$ in the correct orientation (referenced to the activated structure) with respect to the outer domain. TMD runs were performed for 5 ns with a spring constant of 500 kcal $mol^{-1}Å^{-2}$ and with the barostat turned off. To create the target structures, the initial structure was aligned over the corresponding CD4-bound conformation using the outer domain with PDB 2NY0 used for the non-stitched sequence and 2NY5 used for the stitched sequence, respectively. For each TMD run, upon completion, the barostat was turned on and the systems were subjected to 20 ns of equilibration. Finally, in order to examine $\beta 20/\beta 21$ movement in the context of the $\alpha 1$-folded 2NY7 structure, all heavy atoms of this domain were forced back to their crystallographic positions. Since the RMSD values between the starting and end structures is very small and to perform the simulation in a reasonable amount of time, the *k* value for this TMD run was set to 5000 kcal mol^{-1} $Å^{-2}$. Table 1 provides a summary of all simulations.

RESULTS

MD equilibration of DS1 and DS1* gp120

Figure 2 shows domain-specific RMSD for outer-domain-aligned DS1 and DS1* from 20 ns standard MD trajectories. As can be seen in Figure 2a, the DS1 outer domain has a very low value of RMSD which is comparable to the values reported previously for the activated gp120 conformation (22). The DS1 inner domain is also fairly stable, despite α1 lacking the helical structure it has in the activated conformation. Only the backbone W112.N-I108.O hydrogen bond near the C-terminus of α1 is present during the simulation and the rest of the segment lacks secondary structure. β2/β3 was modeled as an unstructured loop (see Methods) and its high RMSD values are therefore not surprising. More interesting is the RMSD trace of the β20/β21 hairpin. As was mentioned before, β20/β21 in the b12-bound structure is not in the same β-hairpin conformation as in the activated state. Carrying one of the building blocks of the functionally critical F43 pocket in the CD4-bound structure, namely the side-chain of W427, β20/β21 is tightly bound to the core of the molecule in the activated state crystal structures (22,23). Despite being covalently linked to α1 in DS1, β20/β21 is flipped and also fairly flexible in the b12-bound conformation. This point is more pronounced in DS1* which lacks the covalent bond stitching β20/β21 to the inner domain. The RMSD traces of DS1* are displayed in Figure 2b. When only the I109C/Q428C mutations are reverted back to wild-type, β20/β21 becomes significantly more mobile, reflected in the RMSD upturn of DS1* β20/β21 after ≈15 ns. The root mean squared fluctuations (RMSF) of C_α atoms in β20/β21 are increased on average by >70% (not shown). Removal of the covalent link also increases the RMSD of the inner domain. Relieving the constraints imposed on α^1 by the stitch to β20/β21 is expected to result in increased conformational freedom which contributes to the increased RMSD of the inner domain in DS1*, so these results are not surprising.

In contrast to the case of DS1, wherein β20/β21 is restrained by α1 and the bottom of α1 is restrained by stitching to β20/β21, in DS1* these two structural elements show large amplitude movements while maintaining their internal structure. In particular, the W112.N-I108.O hydrogen bond of α1 is stable and maintains partial helicity of the C-terminus of α1, while β20/β21 shows very small intradomain RMSD which demonstrates its internal structural stability.

To get a better understanding of the fluctuations in α1 and β20/β21, we measured the distances of both β20/β21 and the C-terminus of α1 from the core of gp120. We used the center of mass of residues 108-112 as representative of the position of C-terminus of α1 and the coordinates of the C_α atom of residue G431 as representative of β20/β21, respectively. The C_α atom of residue S257 was chosen as a representative of the hydrophobic core of gp120. The results are shown in Figure 3. In DS1 the α1 and β20/β21 domains have an almost constant distance from the core of the molecule but toward the end of the simulation, larger fluctuations start to develop in the β20/β21-core distance despite the α1-core distance staying almost constant. In DS1*, the C-terminus of α1 (particularly I108) enters the hydrophobic pocket of residues around the putative F43 pocket temporarily, while β20/β21 stays very close to this area (Figure 4). But when β20/β21 starts to move away from this region (as can be seen from the increase in β20/β21-core distance around 14 ns), α1 moves back to its starting location relative to the core.

Although the movements of the bottom part of α1 in DS1* structure do not seem to result in a significant net change in the orientation of this domain relative to the core, despite its fluctuations, a closer look at the residues in this part of the molecule suggests that the correlated movement of the bottom part of α1 with β20/β21 may result in a rearrangement of these constituents relative to one another. This can be better viewed in light of the change in

residue specific solvent accessible surface area (SASA) and its evolution throughout the trajectory. As a measure of SASA, we use the fractional SASA (FSASA) in which the SASA value computed for each residue is normalized to the value that residue has in a small standard tripeptide (24). A residue is considered buried if FSASA <0.1, somewhat exposed if 0.1 <FSASA <0.4 and fully solvent exposed if FSASA >0.4 (5). From the FSASA trace for the residues 108-112 and 423-435, those that showed significant changes in surface exposure were three hydrophobic residues: I108, I109 and L111. The FSASA trace for these residues is shown in Figure 5 along with W112 as a reference buried residue. In DS1, the FSASA values stay more or less constant with regard to the surface exposure limits defined above, although some decrease in FSASA toward burial (FSASA <0.1) is observed for the hydrophobic side chains of I108 and I109. In contrast, FSASA values behave much differently in the DS1* structure.

Although FSASA fluctuations of I108 are similar to the stitched case, I109 and L111 become much more buried in DS1*. These changes are accommodated by movement of β20/β21 away from the core which leads to exposure of Q428 and burial of I109 and L111. These changes seem to suggest that the disulfide bridge in the b12-bound conformation might have trapped some hydrophobic residues on the unstructured α1 in a solvent exposed state when b12 is bound. This restraint is relaxed when the disulfide bridge is removed and the β20/β21 is allowed to move away from the gp120 hydrophobic core.

Folding the α1 helix using TMD

TMD runs were performed to fold the α1 helix. After folding the helix, the structure was relaxed by equilibration for 20 ns. Figure 6 shows the RMSD trace of the relaxation process. As expected, the outer domain remains fairly stable and most of the relaxation takes place in the inner domain and to some (lesser) degree β20/β21. The intradomain RMSD of α1 shows that the helical structure is fairly stable with the helix as a whole moving slightly relative to the rest of the molecule.

Examining the DS1 and DS1* TMD trajectories, it can be seen that folding of α1 brings β20/β21 closer to the core of the molecule in both cases. To quantify this, the distance between C_α atoms of G431 at the tip of β20/β21 and T257 as a representative of the hydrophobic core around the F43 pocket was measured, and the results are shown in Figure 7. The G431-T257 distance decreases during the TMD run for both cases: for DS1 it decreases from 23.4 to 13.4 Å and for DS1* it decreases from 26.2 to 17 Å. After TMD steering forces are lifted and the structures are left to equilibrate, almost the same difference between the two structures remains: β20/β21 in the stitched DS1 stays closer to the core (≈4 Å closer).

Steric constraints imposed by b12 on the folding of α1 in the “stitched” structure

We have shown that when α1 is folded, the stitch causes β20/β21 to move closer to the core compared with the non-stitched case. This raises the question of whether or not the position of β20/β21 in the stitched α1-folded structure could interfere with the binding of b12. To investigate this, we aligned the gp120 outer domain of the 2NY7 crystal complex over gp120 of the simulation. Repeating this frame-by-frame, after removal of the crystal complex gp120, we produced a combined trajectory in which b12 is overlaid on gp120. To count overlaps, at each frame and after alignment, those heavy atoms of b12 that were closer than 2.0 Å to β20/β21 domain atoms were counted as overlapping atoms. Each pair of overlapping atoms was counted as one overlap. As shown in Figure 8, we observe a drastic difference between the amount of overlap resulting from folding of α1 in the context of the stitched DS1 structure compared to the non-stitched DS1*, with folding of α1 in the stitched case resulting in ≈16 times more total overlaps.

Repositioning β20/β21 with TMD after folding of α1

We have shown here that forcing α1 to fold in DS1 results in strong clash of β20/β21 with an aligned b12. This raises the question whether or not forcing β20/β21 back out of collision with b12 results in unfolding of α1. To test this, we began with the end-point coordinates of the equilibrated, α1-folded DS1 simulation and launched a TMD simulation to force β20/β21 back to its 2NY7 crystal structure position relative to the core.

As is seen from Figure 9, β20/β21 is moving away from the core during TMD, as shown by the G431.C_α-S257.C_α distance. β20/β21 does not reach its target conformation during the 2 ns TMD performed here and stays a bit closer to the core than what is expected. Nevertheless we observe the destruction of at least 5 major backbone hydrogen bonds in the middle of α1, which kinks the helix (Figure 10). We did not perform the same TMD run on DS1* because the end conformation of β20/β21 after TMD of α1 and equilibration is already farther away from the core compared to original 2NY7 crystal structure, so moving β20/β21 to its crystal structure position is equivalent to moving the domain closer to the core. TMD of α1 already showed this will not disrupt α1 folding in DS1*.

Discussion

According to Zhou *et al.*, the DS1* sequence did not yield a b12-bound crystal structure despite lacking only one disulfide linkage compared to DS1, which yielded the 2NY7 structure (10). Successful crystallization was attributed to the reduced flexibility of the molecule which was achieved in part by stitching the α1 and β20/β21 domains together. Our results are in line with the rationale for addition of this key constraint to the gp120 sequence, which seems to significantly affect interdomain fluctuations of various components of the molecule that seem to be necessary for shaping the F43 pocket. In particular, the DS1* mutant shows higher RMSD values for α1 and β20/β21 relative to the rest of the molecule (i.e. core). In its CD4-bound form, the pocket is made up by contributions mainly from the outer domain, W112 of the inner domain and W427 of the β20/β21 strand (5). In all HIV-1 gp120 conformations resolved to date, the outer domain components are conformationally rigid, suggesting that the conformationally labile components of the pocket are contributed by the inner domain and the bridging sheet. The 2NY7 structure shows W112 in relatively close proximity to its activated state position (although tilted) but the highly conserved W427 faces outward and away from the pocket, in contrast to its orientation in all other structures. Analysis of the equilibration run for DS1* suggests that the disulfide bridge is to a large extent responsible for bringing the various hydrophobic residues around the pocket together (although in a different conformation compared to the activated state) and when removed, the free gp120 structure tends to relax at least some of the constraints imposed by the disulfide bridge. This relieving of constraints is explicitly observable through the relaxation of the β20/β21 strand and large fluctuations (≈4 Å) of the α1 domain toward and away from the core (Figure 3). Recently, it was suggested that gp120 is structured in layers which both contribute to its unusual conformational diversity and also mask the functionally important domains from the immune system (25–27). This model suggests a conformationally plastic inner domain. The observations that even in such highly engineered gp120's as those investigated here which are “mutationally stabilized” (10) we see two states of α1 (folded and unfolded) and also the mobility of the C-terminal end of α1 in its unfolded from, are both consistent with the above model.

Among all gp120 conformations resolved to date, only those from the mutagenically stabilized ones in complex with b12 or b13 show an unfolded α1 (8,10). The flipped β20/β21 in these structures (compared to the canonical CD4-bound conformation), the existence of a bridge from β20/β21 to the C-terminus of α1, and the proposed plasticity of the inner domain of gp120 all point to a possible correlation between the existence of the disulfide

link and unfolding of α1 in the engineered mutants. To investigate this hypothesis, we attempted to fold α1 using TMD in both the stitched DS1 structure (2NY7 PDB) and an *in-silico* created mutant lacking the I109C/Q428C mutation (DS1*). The results of folding α1 were analyzed after equilibration of the structure to relax the perturbations introduced by application of TMD forces. The resulting conformations were found to be stable, especially when the helicity of the α domain was considered. This shows that the ensemble of conformations adopted by gp120 when bound to b12 is diverse enough to allow for a folded α1. This is also in line with the proposed plasticity of the inner domain in that it shows both the folded and unfolded α1 are stable (within the time frame of simulation) even in the context of the conformationally stabilized gp120's considered here. These mutants were made to be structurally rigid and yet they still show conformational diversity in the inner domain. It is plausible that in wild-type gp120, with the stabilizing mutations removed, inner domain will be even more flexible, possibly incorporating folding/unfolding transitions of α1.

From the crystal structure of b12-bound gp120, it can be seen that b12 latches on to the CD4 binding loop. Although β20/β21 in DS1 and DS1* is not in its activated state conformation, folding of α1 moves β20/β21 closer to the core of the molecule in the stitched structure of DS1 because of the disulfide bridge, since this movement is less profound in DS1* . When combined with the stability of the folded α1 in both structures, one arrives at the conclusion that when β20/β21 is coupled to α1 through the disulfide bridge, binding of b12 and the slight “push” it exerts on β20/β21 may favor the unfolded state of α1 in these engineered mutants. We were interested to see whether simple steric constraints support this conclusion or not. When b12 is ovelayed on the TMD runs, it can be seen that the TMD run of DS1 produces a large amount of steric overlap which when combined with the β20/β21-core metric, suggests that movement of β20/β21 away from the core is required for b12 binding. It was found that DS1* has almost a four fold larger on-rate for binding of b12, relative to DS1 which yielded the 2NY7 structure (compare DS1F123 and DS12F123 sequences in reference (10)). This provides support to our finding that in DS1, the tighter association of β20/β21 with the core provides a smaller window of opportunity for b12 to bind, considering the natural movements of β20/β2α toward and away from the core observed in both DS1 and DS1* equilibrations. Also, these data suggest that stabilized gp120 is flexible enough to allow for a folded α in the context of the b12-bound conformation, but when the I109C/Q428C stitch is introduced in the sequence, the resulting coupling of α1 and β20/β21 movement helps b12 translate its influence on β20/β21 conformation to α1, which may favor its unfolding.

Finally, to directly test this idea, we used TMD to reposition β20/β21 back to its crystallographic position in α1-folded DS1 and observed that indeed α1 starts to unfold. This lends support to our hypothesis that although a folded α1 is stable in both the disulfide-stitched and non-stitched structures, movement of stitched β20/β21 away from the core to make room for binding of b12 can displace the equilibrium between the folded and unfolded α1 in favor of the unfolded state in stabilized gp120's studied here.

Conclusions

We have used MD and TMD simulations to show that introduction of the I109C/Q428C disulfide bridge between the α1 helix and β20/β21 in an engineered HIV-1 gp120 leads to coupling of the natural fluctuations of the two domains and limits their mobility, especially restricting the motions of β20/β21 away from the core of the molecule and the hydrophobic patch of residues around the F43 pocket. Additionally we used targeted molecular dynamics to fold α1 both with and without the disulfide stitch. Our results suggest that a conformation with α1 folded is stable both in the presence and absence of the disulfide stitch. We find

such a conformational plasticity of α1 even in the stabilized mutants, consistent with recent findings suggesting a conformationally plastic inner domain in wild-type gp120 (26). Folding α1 forces β20/β21 closer to the core of the molecule in the disulfide stitched mutant. When b12 is overlaid on such a conformation, a significantly larger number of atoms overlap between b12 and gp120. These overlaps suggest that binding of b12 and subsequent pushing of β20/β21 away from the core, possibly coupled with the pocket-filling mutations which stabilize the bottom part of α1 close to the core, may contribute to α1 unfolding. To support this, we pushed β20/β21 away from the core in the α1 folded state of the b12-bound conformation and observed that indeed such a movement of β20/β21 leads to unfolding of α1. These results suggest that although b12 does not contact the inner domain, its effect on the conformation of β20/β21 (compared with the CD4-bound state) is transmitted to α1 through the disulfide bridge of I109C/Q428C. This was not observed when the disulfide bridge was removed. Therefore, in the absence of such a stitching disulfide, α1 may be able to shuttle freely between folded and unfolded states, even when b12 is bound. This provides an alternative picture of b12-bound gp120 and can be used for better design of engineered gp120 constructs which might be used as improved immunogens (2).

Acknowledgments

This work was supported by NSF Grant DMR-042763 and TeraGrid allocation MCB070073N.

References

1. Poignard P, Saphire E, Parren P, Burton D. Gp120: Biologic aspects of structural features. Annu Rev Immunol. 2001; 19:253–274. [PubMed: 11244037]
2. Phogat S, Wyatt R. Rational modifications of hiv-1 envelope glycoproteins for immunogen design. Curr Pharm Design. 2007; 13:213–227.
3. Wyatt R, Sodroski J. The hiv-1 envelope glycoproteins: Fusogens, antigens, and immunogens. Science. 1998; 280:1884–1888. [PubMed: 9632381]
4. Weiss C, Levy J, White J. Oligomeric organization of gp120 on infectious human-immunodefficiency-virus type-1 particles. J Virol. 1990; 64:5674–5677. [PubMed: 2214033]
5. Kwong P, Wyatt R, Robinson J, Sweet R, Sodroski J, Hendrickson W. Structure of an hiv gp120 envelope glycoprotein in complex with the cd4 receptor and a neutralizing human antibody. Nature. 1998; 393:648–659. [PubMed: 9641677]
6. Kwong P, Wyatt R, Majeed S, Robinson J, Sweet R, Sodroski J, Hendrickson W. Structures of hiv-1 gp120 envelope glycoproteins from laboratory-adapted and primary isolates. Structure. 2000; 8:1329–1339. [PubMed: 11188697]
7. Huang C, Tang M, Zhang M, Majeed S, Montabana E, Stanfield R, Dimitrov D, Korber B, Sodroski J, Wilson I, Wyatt R, Kwong P. Structure of a v3-containing hiv-1 gp120 core. Science. 2005; 310:1025–1028. [PubMed: 16284180]
8. Chen L, Kwon YD, Zhou T, Wu X, O'Dell S, Cavacini L, Hessell AJ, Pancera M, Tang M, Xu L, Yang ZY, Zhang MY, Arthos J, Burton DR, Dimitrov DS, Nabel GJ, Posner MR, Sodroski J, Wyatt R, Mascola JR, Kwong PD. Structural basis of immune evasion at the site of cd4 attachment on hiv-1 gp120. Science. 2009; 326:1123–1127. [PubMed: 19965434]
9. Myszka D, Sweet R, Hensley P, Brigham-Burke M, Kwong P, Hendrickson W, Wyatt R, Sodroski J, Doyle M. Energetics of the hiv gp120-cd4 binding reaction. P Natl A Sci USA. 2000; 97:9026–9031.
10. Zhou T, Xu L, Dey B, Hessell AJ, Van Ryk D, Xiang SH, Yang X, Zhang MY, Zwick MB, Arthos J, Burton DR, Dimitrov DS, Sodroski J, Wyatt R, Nabel GJ, Kwong PD. Structural definition of a conserved neutralization epitope on hiv-1 gp120. Nature. 2007; 445:732–737. [PubMed: 17301785]
11. Chen B, Vogan E, Gong H, Skehel J, Wiley D, Harrison S. Structure of an unliganded simian immunodeficiency virus gp120 core. Nature. 2005; 433:834–841. [PubMed: 15729334]

12. Kwong P, Doyle M, Casper D, Cicala C, Leavitt S, Majeed S, Steenbeke T, Venturi M, Chaiken I, Fung M, Katinger H, Parren P, Robinson J, Van Ryk D, Wang L, Burton D, Freire E, Wyatt R, Sodroski J, Hendrickson W, Arthos J. Hiv-1 evades antibody-mediated neutralization through conformational masking of receptor-binding sites. Nature. 2002; 420:678–682. [PubMed: 12478295]

13. Bublil EM, Yeger-Azuz S, Gershoni JM. Computational prediction of the cross-reactive neutralizing epitope corresponding to the monoclonal antibody b12 specific for hiv-1 gp120. FASEB J. 2006; 20:1762–1774. [PubMed: 16940148]

14. Phillips J, Braun R, Wang W, Gumbart J, Tajkhorshid E, Villa E, Chipot C, Skeel R, Kale L, Schulten K. Scalable molecular dynamics with namd. J Comput Chem. 2005; 26:1781–1802. [PubMed: 16222654]

15. MacKerell A, Feig M, Brooks C. Extending the treatment of backbone energetics in protein force fields: Limitations of gas-phase quantum mechanics in reproducing protein conformational distributions in molecular dynamics simulations. J Comput chem. 2004; 25:1400–1415. [PubMed: 15185334]

16. MacKerell A, Bashford D, Bellott M, Dunbrack R, Evanseck J, Field M, Fischer S, Gao J, Guo H, Ha S, Joseph-McCarthy D, Kuchnir L, Kuczera K, Lau F, Mattos C, Michnick S, Ngo T, Nguyen D, Prodhom B, Reiher W, Roux B, Schlenkrich M, Smith J, Stote R, Straub J, Watanabe M, Wiorkiewicz-Kuczera J, Yin D, Karplus M. All-atom empirical potential for molecular modeling and dynamics studies of proteins. J Phys Chem B. 1998; 102:3586–3616.

17. Jorgensen W, Chanderasekhar J, Madura J, Impey R, Klein M. Comparison of simple potential functions for simulating liquid water. J Chem Phys. 1983; 79:926–935.

18. Andersen HC. Rattle: A velocity version of the shake algorithm for molecular dynamics calculations. J Comput Phys. 1983; 52:241–34.

19. Martyna G, Tobias D, Klein M. Constant-pressure molecular-dynamics algorithms. J Chem Phys. 1994; 101:4177–4189.

20. Feller S, Zhang Y, Pastor R, Brooks B. Constant-pressure molecular-dynamics simulation - the langevin piston method. J Chem Phys. 1995; 103:4613–4621.

21. Schlitter J, Engels M, Kruger P. Targeted molecular-dynamics - a new approach for searching pathways of conformational transitions. J Mol Graphics. 1994; 12:84–89.

22. Pan Y, Ma B, Keskin O, Nussinov R. Characterization of the conformational state and flexibility of hiv-1 glycoprotein gp120 core domain. J Biol Chem. 2004; 279:30523–30530. [PubMed: 15131118]

23. Pan Y, Ma B, Nussinov R. Cd4 binding partially locks the bridging sheet in gp120 but leaves the beta 2/3 strands flexible. J Mol Biol. 2005; 350:514–527. [PubMed: 15946678]

24. Chothia C. The nature of the accessible and buried surfaces in proteins. J Mol Biol. 1976; 105:1–14. [PubMed: 994183]

25. Xiang SH, Finzi A, Pacheco B, Alexander K, Yuan W, Rizzuto C, Huang CC, Kwong PD, Sodroski J. A v3 loop-dependent gp120 element disrupted by cd4 binding stabilizes the human immunodeficiency virus envelope glycoprotein trimer. J Virol. 2010; 84:3147–3161. [PubMed: 20089638]

26. Finzi A, Xiang SH, Pacheco B, Wang L, Haight J, Kassa A, Danek B, Pancera M, Kwong PD, Sodroski J. Topological layers in the hiv-1 gp120 inner domain regulate gp41 interaction and cd4-triggered conformational transitions. Moll Cell. 2010; 37:656–667.

27. Panceraa M, Majeed S, Andrew YE, Chen L, Huang Cc, Kong L, Kwon YD, Stuckey J, Zhoua T, Robinson JE, Schief WR, Sodroski J, Wyatt R, Kwong PD. Structure of hiv-1 gp120 with gp41-interactive region reveals layered envelope architecture and basis of conformational mobility. P Natl A Sci USA. 2010; 107:1166–1171.

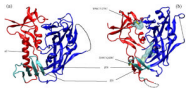

FIG. 1.

(a) CD4-bound (PDB 1GC1) and **(b)** b12-bound (PDB 2NY7) conformations of gp120. The inner domain is red, outer domain blue and the bridging sheet cyan. In (b) licorice rendering shows the two disulfide bridges (hydrogen atoms not shown) between the inner and outer domain and the residues shown in transparent van der Waals are the other stabilizing mutations (M95W, T257S, S375W, A433M). The dashed lines show the unresolved V4 domain in both structures and also parts of the $\beta 2/\beta 3$ domain and base of the V1/V2 loop in the b12-bound conformation.

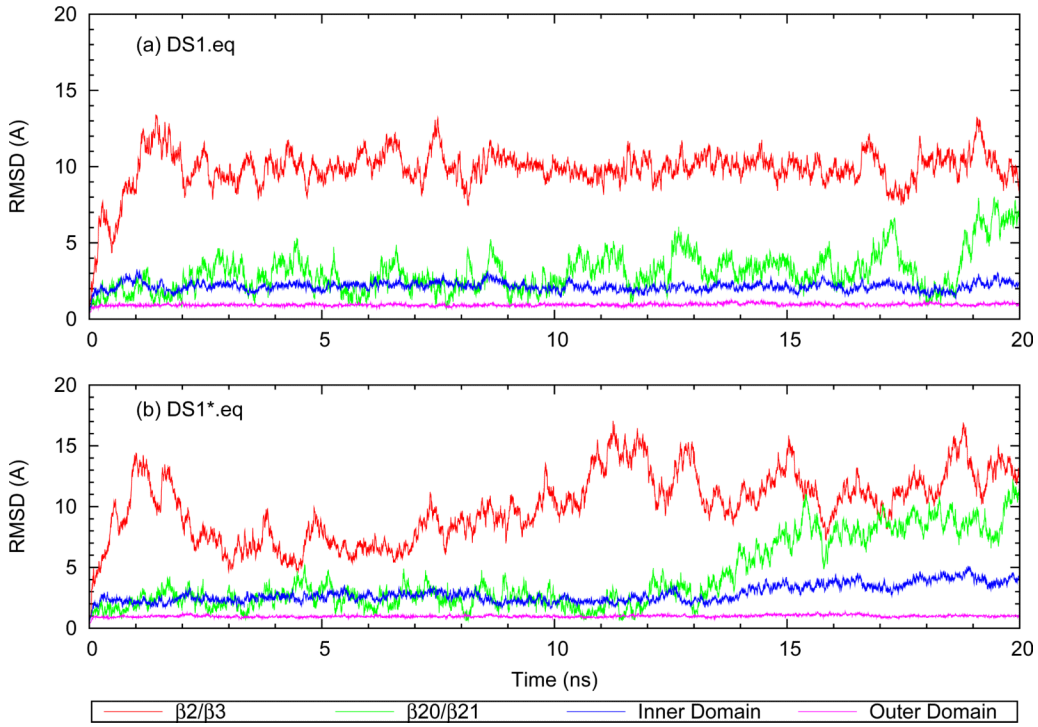

FIG. 2.

C_α RMSD trace of different gp120 domains after alignment using the outer domain: **(a)** disulfide-"stitched" structure **(b)** non-stitched structure.

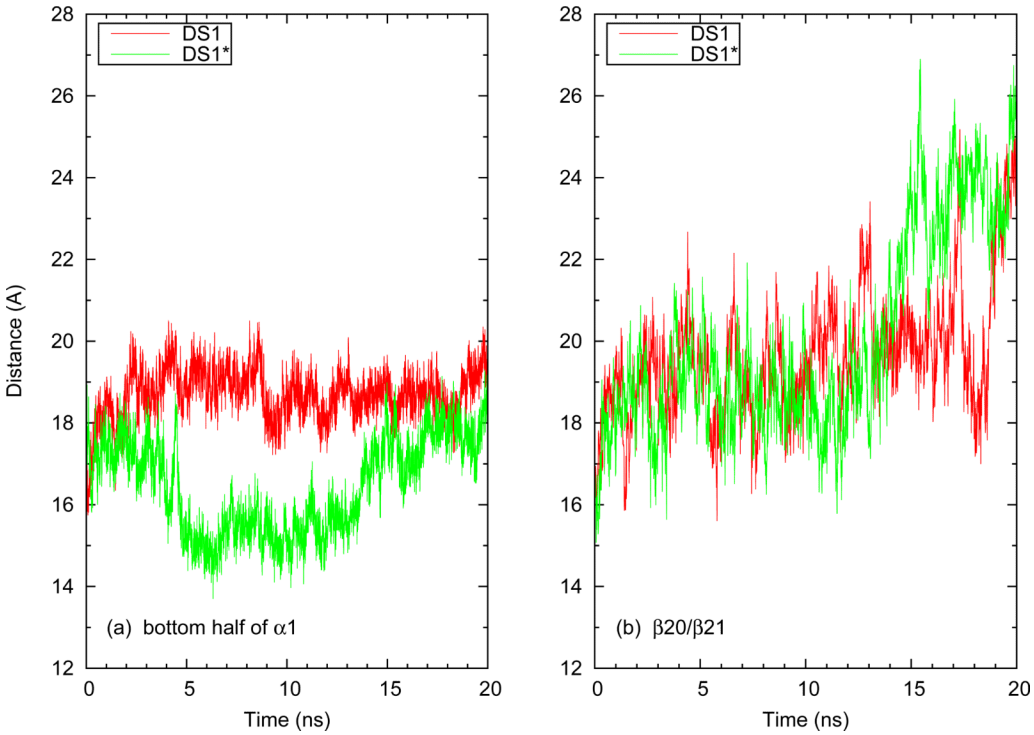

FIG. 3.

Distance of (a) α1 and (b) β20/β21 from the C_α atom of core residue S257 during equilibration of DS1 and DS1*. β20/β21 is represented by the C_α atom of residue G431 at its tip. α1 is represented by the center of mass of residues 108-112.

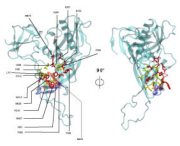

FIG. 4.

Hydrophobic residues in and around the putative F43 pocket in the DS1* structure. Residues in red make up the F43 pocket (5). Residues shown in yellow are hydrophobic residues within 10 Å of residue 382 and taken to be close to the pocket. The position of the β20/β21 domain at the beginning (red) and end (blue) of the DS1* equilibration is shown in cartoon rendering.

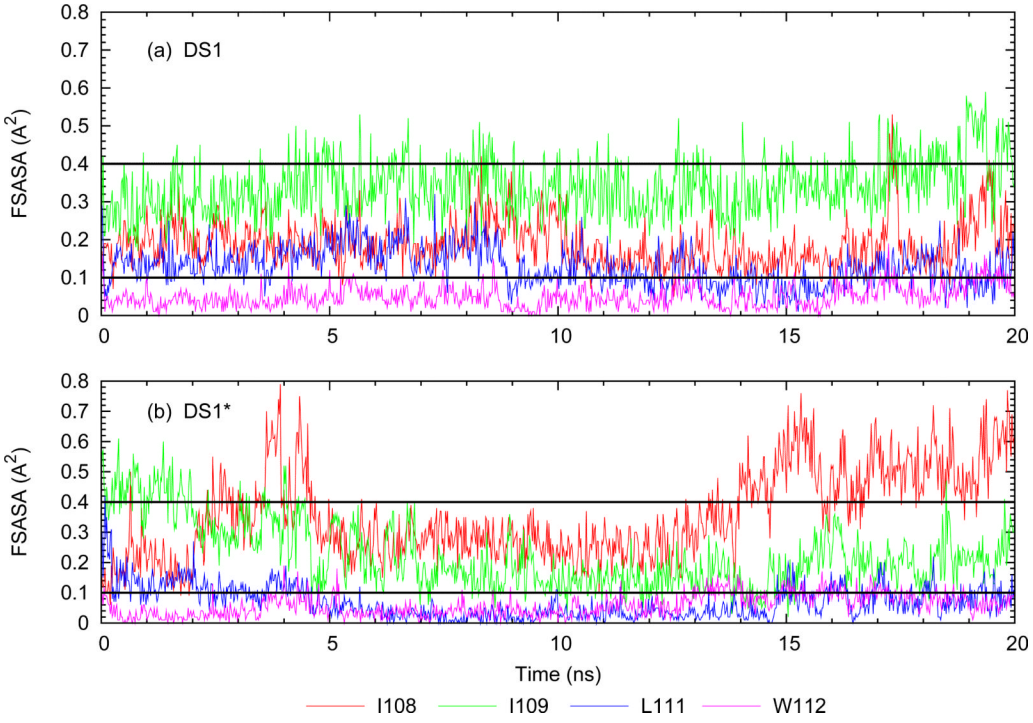

FIG. 5.

Evolution of fractional surface accessible area (FSASA) for residues at the bottom of α1. The dashed lines at 0.1 and 0.4 show the limiting values for definition of buried and exposed residues.

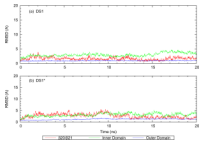

FIG. 6.

Equilibrium backbone RMSD evolution after removal of the TMD forces. Each frame in the trajectory is aligned over the first frame of equilibration (i.e. last frame of TMD forcing) using the outer domain backbone (details explained in the previous section).

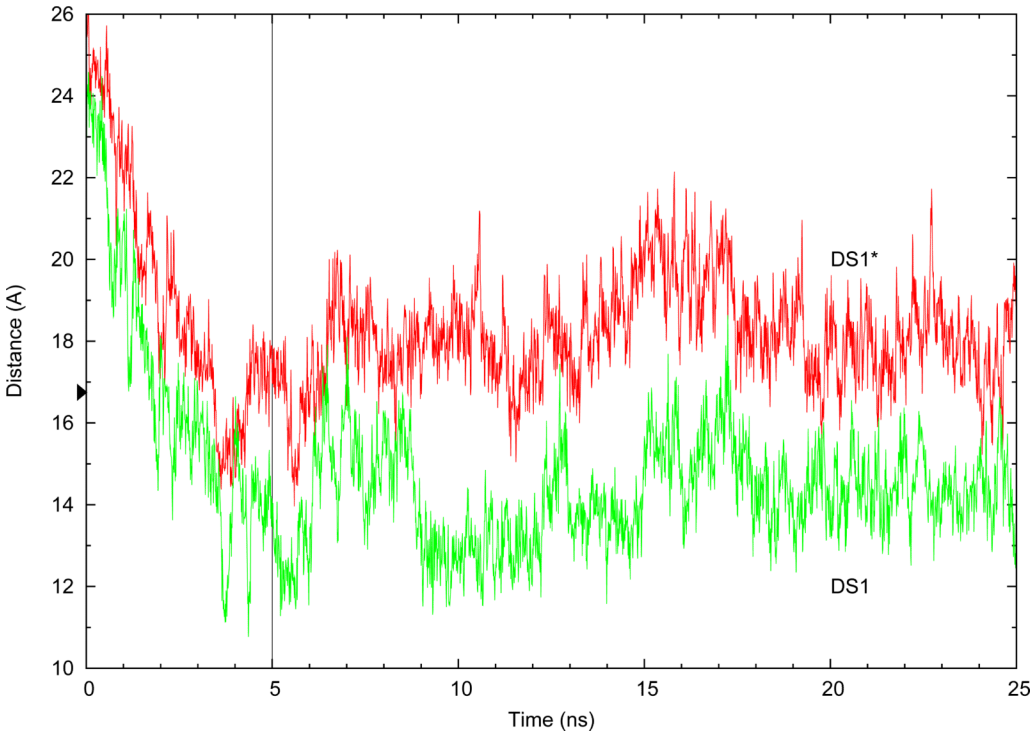

FIG. 7.

Movements of the β20/β21 strand relative to the core as measured by the distance G431.CA-T257.CA, during TMD and post-TMD equlibrations. The small arrow at 16.95 Å shows the value of the metric in the CD4-bound crystal structure (1GC1) of gp120. The vertical line indicates the transition from TMD to equilibration.

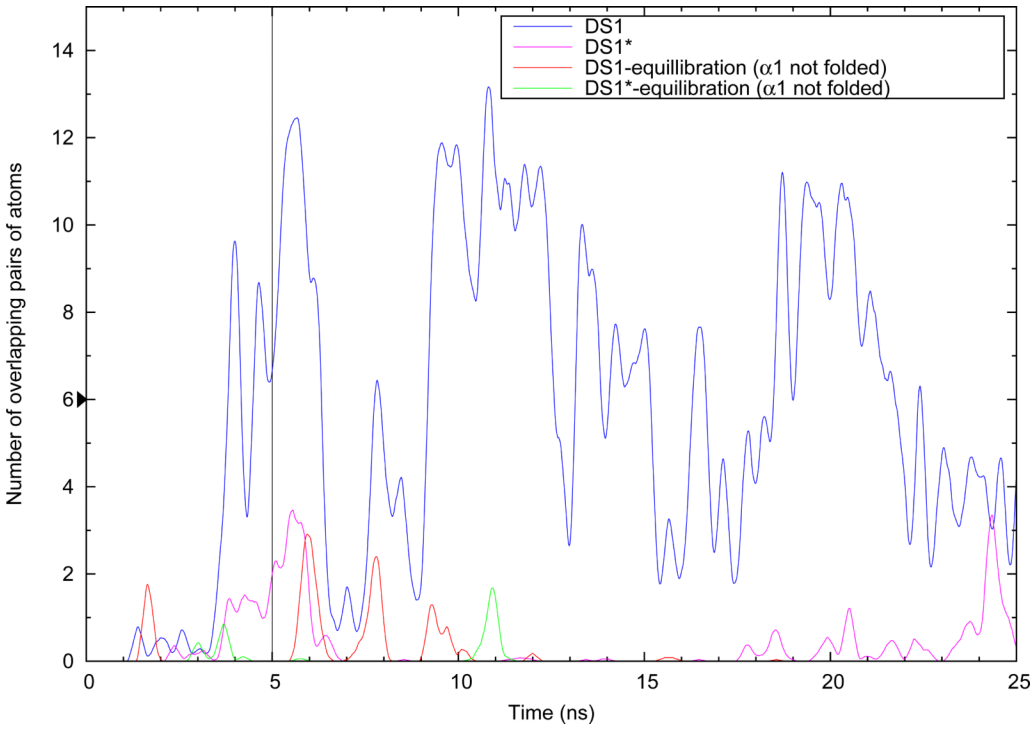

FIG. 8.

Number of overlapping pairs of atoms resulting from overlaying b12 on α1-folded gp120. The raw data were smoothed using a triangular average method with a sampling window size of 0.5 ns. The vertical line indicates where the TMD forces are lifted and equilibration is started. The small arrow at n=6 overlaps shows the number of overlaps generated when using gp120 extracted the CD4-bound crystal structure (PDB 1GC1).

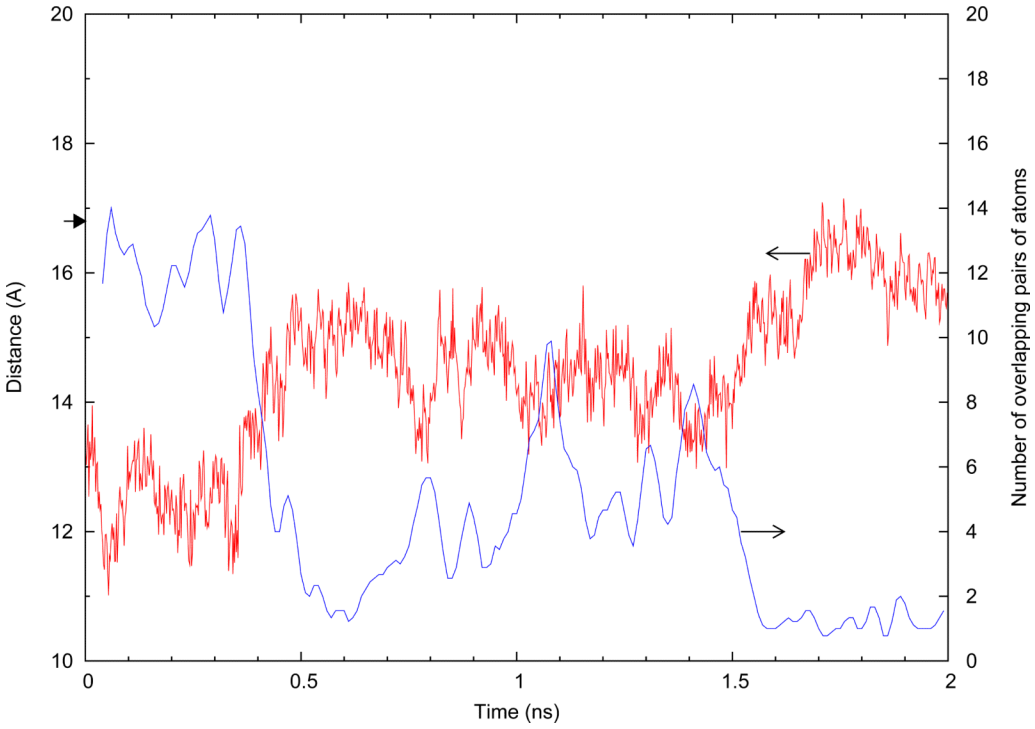

FIG. 9.

Distance between C_α atoms of G431 and S257 when β20/β21 is repositioned. The small arrow at 16.8 Å indicates this distance in the 2NY7 crystal structure of stitched gp120. Also plotted, is the number of b12/gp120 overlaps (smoothed with a sampling window size of 0.02 ns).

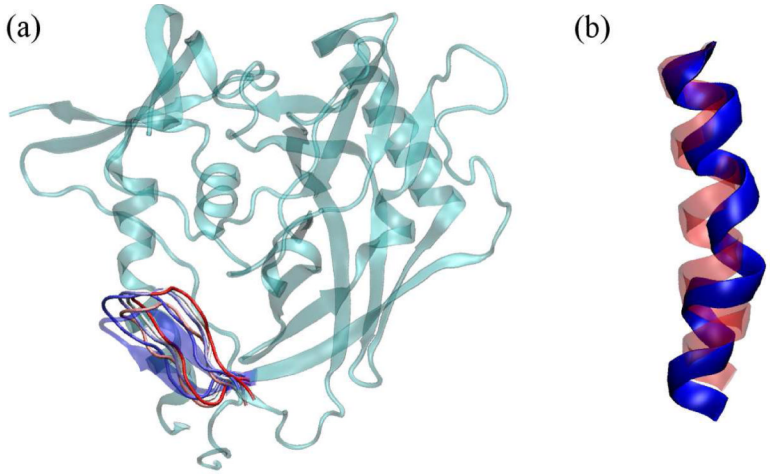

FIG. 10.

(a) Schematic representation of how β20/β21 was moved when it was pushed away from the hydrophobic core in DS1. Representative frames with a sampling rate of 1 frame per 0.5 ns are shown in tube rendering with the starting state in red and the final state in blue (only the β20/β21 region is depicted, the coordinates of the rest of the molecule are from the starting frame). β20/β21 from the crystal structure is shown in blue cartoon rendering. **(a)** α1 helix conformation during the TMD run with red showing the domain in the beginning and blue in the end of the simulation. At least 5 hydrogen bonds are destroyed.

TABLE I

Summary of the runs discussed in this work.

Designation	Explanation
DSl.eq	equilibration (20 ns) of the bl2-bound conformation of the stitched gpl20 mutant
DSl*.eq	equilibration (20 ns) of the bl2-bound conformation with the I109C/Q428C mutation removed
DSl.tmd	all-heavy-atom folding (5 ns) of α1 in DS1 followed by equilibration (20ns)
DSl*.tmd	all-heavy-atom folding (5 ns) of α1 in DS1* followed by equilibration (20ns)
DSl.b20b21	After equilibration of DSl.tmd run, β20/β21 is moved back to its crystal structure state (2 ns)